Enabling Communication via Automotive Radars: An Adaptive Joint Waveform Design Approach

Ceyhun D. Ozkaptan, Eylem Ekici
Dept. of Electrical and Computer Engineering
The Ohio State University
Columbus, OH, USA
ozkaptan.1@osu.edu, ekici.2@osu.edu

Onur Altintas
InfoTech Labs,
Toyota Motor North America R&D
Mountain View, CA, USA
onur.altintas@toyota.com

***Abstract*—Large scale deployment of connected vehicles with cooperative sensing technologies increases the demand on the vehicular communication spectrum in 5.9 GHz allocated for the exchange of safety messages. To support high data rates needed by such applications, the millimeter-wave (mmWave) automotive radar spectrum at 76-81 GHz can be utilized for communication. For this purpose, joint automotive radar-communication (JARC) system designs have been proposed in the literature to perform both functions using the same waveform. However, employing a large band in the mmWave spectrum deteriorates the performance of both radar and communication functions due to frequency-selectivity. In this paper, we address the optimal joint waveform design problem for wideband JARC systems via Orthogonal Frequency-Division Multiplexing (OFDM). We show that the problem is a non-convex quadratically constrained quadratic fractional programming (QCQFP) problem, which is known to be NP-hard. Existing approaches to solve QCQFP include Semidefinite Relaxation (SDR) and randomization approaches, which have high time complexity. Instead, we propose an approximation method to solve QCQFP more efficiently by leveraging structured matrices in the quadratic fractional objective function. Finally, we evaluate the efficacy of the proposed approach through numerical results.**

I. Introduction

As an integral part of Intelligent Transportation Systems (ITS), the connected vehicle technology will promote safer and coordinated transportation through wireless communication and sensing. To enable vehicle-to-vehicle (V2V) and vehicle-to-infrastructure (V2I) communication with low-latency, Dedicated Short-Range Communication (DSRC) has been designed for the exchange of safety messages in the 5.9 GHz spectrum with 75 MHz bandwidth [1]. As an alternative, Cellular-V2X (C-V2X) has been designed for vehicular communication based on Long-Term Evolution (LTE) that provides both cellular and direct communication interfaces for V2I and V2V, respectively [2].

With the deployment of connected vehicles and the intelligent infrastructure at a larger scale, the 5.9 GHz spectrum will face a spectrum scarcity problem due to its limited bandwidth. In addition, emerging cooperative sensing and autonomous driving technologies require a large amount of raw sensor and navigation data to be exchanged for improved reliability and performance [3], [4]. Hence, the allocated spectrum cannot be used efficiently for larger payloads and non-safety related data along with high priority basic safety messages. A solution to alleviate the scarcity problem and attain higher data rates is to leverage the underutilized millimeter-wave spectrum (mmWave) with larger allocated bandwidth.

Currently, 76-77 GHz and 77-81 GHz mmWave spectra are allocated for the automotive long-range radar (LRR) and short-range/medium-range radar (SRR/MRR) with bandwidths of 1 and 4 GHz, respectively [5]. Higher bandwidth and smaller wavelength at mmWave enable better radar sensing resolution and accuracy in terms of range, velocity, and angle. The decrease in wavelength also allows smaller size antenna arrays suitable for automotive systems. As larger bandwidth is required by both communication and radar systems to achieve higher data rate and better sensing accuracy, the most direct solution is the spectral isolation of two systems via regulations. Moreover, interference mitigation and avoidance schemes have been studied in the literature to allow co-existence [6], [7].

As an alternative, joint radar and communication systems have been proposed to eliminate mutual interference by using the same waveform for both radar sensing and data transmission [8]–[11]. Employing such a joint system promotes effective utilization of the spectrum while reducing cost and hardware size. In these works, radar channels are modeled with *simple point targets* and *independent Gaussian noise-like clutter*. The point target model can be valid for far-field targets with narrowband radar transmission. However, wideband radar signal resolves the multiple reflectors on vehicles that are located close to the transmitter in traffic [12]. Similar to frequency-selectivity observed in multi-tap communication channels, radar targets also act as frequency-selective channels against wideband signals. Correspondingly, actual clutters are signal-dependent and modeled with non-flat frequency response as they comprise of unwanted reflections (e.g., road clutter) [13]. Combined with the reflections from the signal-dependent clutter, the frequency-selectivity deteriorates the radar detection and estimation performance [14].

Due to their robustness against frequency-selectivity, Orthogonal Frequency-Division Multiplexing (OFDM) waveforms are suitable for adaptive joint automotive radar-communication (JARC) systems for simultaneous data transmission and radar sensing. The subcarrier coefficients of OFDM pulses can be optimized regarding the frequency-selectivity of both radar and communication channels. With

an adaptive approach, the radar performance can be improved by designing the waveform based on *the extended target response* and mitigating the effect of *signal dependent clutter*. Considering radar and communication requirements, the optimal OFDM waveform generated adaptively for the dual-use transmission system can outperform the single carrier and non-adaptive approaches.

The waveform design problems have been studied in literature for various performance constraints [15], [16]. In [15], radar code is designed to improve the detection performance of radar under similarity and unit modulus constraints. In [16], a joint OFDM waveform design problem is studied to increase reflected signal power under interference and autocorrelation shape constraints. However, designed complex weights impede the operation of phase-shift modulation schemes. In these studies, the optimization problems are formulated as non-convex quadratic programming problems and recast as convex semidefinite programming (SDP) problems by dropping *the non-convex rank-one constraint*. While relaxed SDP problems are solved by interior-point algorithms in polynomial time, the time complexity is still high and increases exponentially with the number of variables. Moreover, the obtained solution is near-optimal due to the relaxation of the rank-one constraint.

In this work, we formulate our problem as a non-convex Quadratically Constrained Quadratic Fractional Programming (QCQFP) problem and propose an approach to solve it with *lower time complexity* by exploiting the Toeplitz structures in the objective function. We also apply the SDP formulation to our problem to compare the time complexity and achieved objective values with the proposed method. The remainder of this paper is organized as follows: In Section II, we define the system model by formulating the dual-use wideband OFDM signal along with radar and communication channels. In Section III, we formulate the optimization problem to design the OFDM waveform based on given metrics. In Section IV, we cast the problem as a convex SDP problem by dropping the non-convex constraint. In Section V and VI, we propose approximation methods to solve the non-convex QCQFP problem with lower time complexity. We present numerical results for the proposed methods in Section VII and conclude our work in Section VIII.

***Notations**:* Boldface lower-case letters denote column vectors $\mathbf{a}$, boldface upper-case letters denote matrices $\mathbf{A}$, and plain lower-case letters denote scalars a. a_i represents the i^{th} element of the vector $\mathbf{a}$. $\mathbb{R}$, $\mathbb{C}$, and $\mathbb{H}$ define the sets of real numbers, complex numbers, and Hermitian matrices, respectively. The superscripts $(\cdot)^T$, $(\cdot)^*$, $(\cdot)^\dagger$, and $(\cdot)^\odot$ denote the transpose, the complex conjugate, the transpose conjugate, and the Hadamard power, respectively. $\mathsf{tr}(\cdot)$, $\mathsf{arg}(\cdot)$, $|\cdot|$, $\|\cdot\|$, and $\|\cdot\|_F$ denote the trace operator, the argument of a complex number, the absolute value, the Euclidean norm, and the Frobenius norm, respectively. $\odot$ represents the Hadamard product operator. The operator $\mathsf{diag}(\mathbf{A})$ returns a vector with diagonal entries of $\mathbf{A}$ input and the operator $\mathsf{Diag}(\mathbf{a})$ returns a diagonal square matrix with the elements of $\mathbf{a}$.

II. System Model

A. Signal Model

The dual-use radar and communication system transmits an OFDM pulse in each pulse repetition interval (PRI) carrying communication symbols modulated with phase-shift keying (PSK). After the transmission of P pulses, the radar receiver processes the reflected pulses by pulse-Doppler processing to generate the range-Doppler map of the illuminated environment. The transmitted baseband OFDM pulse with N subcarriers denoted as $\tilde{\mathbf{x}} = [\tilde{x}_1 \dots \tilde{x}_N] \in \mathbb{C}^{N\times 1}$ in time domain and it is generated by precoding symbols with the inverse discrete Fourier transform (IDFT) as

$$\tilde{\mathbf{x}} = \mathbf{W}_N^\dagger \mathbf{x}, \tag{1}$$

where $\mathbf{W}_N \in \mathbb{C}^{N\times N}$ is the unitary DFT matrix for the N-point Fourier Transform and $\mathbf{x} \in \mathbb{C}^{N\times 1}$ is the OFDM signal in frequency domain. Elements in $\mathbf{x}$ correspond to complex symbols in subcarriers and it is expressed as

$$\mathbf{x} = \mathbf{a} \odot \mathbf{s} = \mathsf{Diag}(\mathbf{s})\mathbf{a}, \tag{2}$$

where $\mathbf{a} \in \mathbb{C}^{N\times 1}$ is the subcarrier coefficients, and $\mathbf{s} \in \mathbb{C}^{N\times 1}$ is the modulated symbols comprised of N_p pilot symbols and N_d data symbols. The transmitted symbols s is formulated as

$$\mathbf{s} = \boldsymbol{\mathcal{P}}_p \mathbf{p} + \boldsymbol{\mathcal{P}}_d \mathbf{d}, \tag{3}$$

where $\mathbf{p} = [p_1, p_2, ..., p_{N_p}]^T$ is pilot symbols, $\mathbf{d} = [d_1, d_2, ..., d_{N_d}]^T$ is data symbols. $\boldsymbol{\mathcal{P}}_p \in \{0,1\}^{N\times N_p}$ and $\boldsymbol{\mathcal{P}}_d \in \{0,1\}^{N\times N_d}$ are the permutation matrices for the placement of pilot and data symbols in the frequency domain, respectively. Every column of $\boldsymbol{\mathcal{P}}$ contains exactly single 1, and the row index of each 1 indicates the index of the corresponding symbol in $\mathbf{s}$. Thus, the OFDM signal in frequency domain is formulated as

$$\mathbf{x} = \boldsymbol{\mathcal{P}}_p \mathbf{x}_p + \boldsymbol{\mathcal{P}}_d \mathbf{x}_d, \tag{4}$$

where $\mathbf{x}_p = \mathbf{a}_p \odot \mathbf{p}$ and $\mathbf{x}_d = \mathbf{a}_d \odot \mathbf{d}$. So, $\mathbf{a}_p$ and $\mathbf{a}_d$ are the subcarrier coefficients for pilot and data symbols, respectively. In matrix form, they are $\mathbf{a}_p = \boldsymbol{\mathcal{P}}_p^T \mathbf{a}_x$ and $\mathbf{a}_d = \boldsymbol{\mathcal{P}}_d^T \mathbf{a}_x$.

B. Target and Clutter Model

For the narrowband signal model, the multiple scatterers on a target are not resolved in range, so their response is contained in a single range cell. Thus, the point target assumption is appropriate to model the response of the targets for narrowband radar signals. However, transmitting a signal with a very large bandwidth reduces the size of each range cell (i.e., improves range resolution). Thus, the response of the target *extends* to several range cells. Therefore, the point target assumption fails to model the response of the target with multiple scatterers as the wideband radar signal resolves each scatterer in range with high range resolution. Similar to multipath propagation in a communication channel, the extended target acts like a frequency-selective channel and is represented with a complex finite impulse response (FIR) vector denoted by $\mathbf{g} \in \mathbb{C}^{L\times 1}$, where L is the order of target's

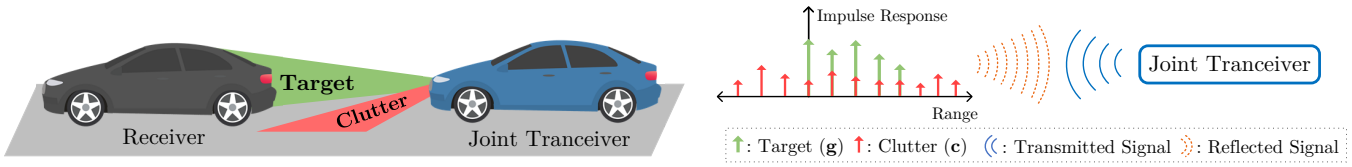

(a) (b)

Fig. 1. (a) The operation of the joint communication and radar system on a vehicle (Blue) which receives reflections from both the target vehicle (Black) and clutter while transmitting data. (b) An illustration of discrete radar operation with reflections from an extended target and clutter.

FIR. The exact knowledge of $\mathbf{g}$ is not attainable in practice, because it varies due to changes in the target's orientation and alignment. Therefore, the target FIR is modeled as a zero-mean circularly symmetric complex Gaussian vector with covariance $\mathbf{\Sigma}_g \in \mathbb{H}^L$ which is obtained as prior information.

Since the response of the target spans L range cells, $M = N + L - 1$ samples are taken in each observation window to be filtered by the receive filter as investigated in [17]. In the range cells of interest, where the target is located, the dominant scatterers are from the target. However, reflections from unwanted scatterers (e.g., road reflections) and reverberation are also received in the same range cells along with the target's response as shown in [17]. These reflections are known as clutter and modeled with a random FIR vector denoted by $\mathbf{c} \in \mathbb{C}^{K\times 1}$, where $K = M + N - 1$ is the order of clutter FIR. The length of clutter is defined as the sum of observation window length and the signal length.

The received discrete baseband signal is denoted by $\tilde{\mathbf{y}} \in \mathbb{C}^{M\times 1}$ and it is the sum of the reflected signals from the target $\tilde{\mathbf{y}}_g$ and clutter $\tilde{\mathbf{y}}_c$ plus the additive noise component $\tilde{\mathbf{n}}$. The reflected signal from the target which is denoted $\tilde{\mathbf{y}}_g$ is formulated as

$$\tilde{\mathbf{y}}_g = g_1 \begin{bmatrix} \tilde{x}_1 \\ \tilde{x}_2 \\ \vdots \\ \tilde{x}_N \\ \mathbf{0}_{L-1} \end{bmatrix} + g_2 \begin{bmatrix} 0 \\ \tilde{x}_1 \\ \vdots \\ \tilde{x}_N \\ \mathbf{0}_{L-2} \end{bmatrix} + \cdots + g_L \begin{bmatrix} \mathbf{0}_{L-1} \\ \tilde{x}_1 \\ \tilde{x}_2 \\ \vdots \\ \tilde{x}_N \end{bmatrix}., \tag{5}$$

where $\mathbf{0}_L$ is a vector with L zeros. Similarly, the reflection from the clutter, which is denoted by $\tilde{\mathbf{y}}_c$, is formulated as

$$\begin{aligned} \tilde{\mathbf{y}}_c = {} & c_{-N+1} \begin{bmatrix} \tilde{x}_N \\ 0 \\ \vdots \\ 0 \end{bmatrix} + c_{-N+2} \begin{bmatrix} \tilde{x}_{N-1} \\ \tilde{x}_N \\ \vdots \\ 0 \end{bmatrix} + \cdots \\ & + c_0 \begin{bmatrix} \tilde{x}_1 \\ \tilde{x}_2 \\ \vdots \\ \tilde{x}_N \\ \mathbf{0}_{L-1} \end{bmatrix} + c_1 \begin{bmatrix} 0 \\ \tilde{x}_1 \\ \vdots \\ \tilde{x}_N \\ \mathbf{0}_{L-2} \end{bmatrix} + \cdots + c_{M-1} \begin{bmatrix} 0 \\ 0 \\ \vdots \\ 0 \\ \tilde{x}_1 \end{bmatrix}. \end{aligned} \tag{6}$$

The components of the received signal in (5) and (6) are the output of linear convolution operation that are received in the observation window. Thus, the observation window contains the targets response along with the clutter response with delayed signals. In matrix form, the received wideband signal $\tilde{\mathbf{y}}$ in the observation window is formulated as

$$\tilde{\mathbf{y}} = \mathbf{T}_g \tilde{\mathbf{x}} + \mathbf{T}_c \tilde{\mathbf{x}} + \tilde{\mathbf{n}}, \tag{7}$$

where $\mathbf{T}_g \in \mathbb{C}^{M\times N}$ is a lower triangular Toeplitz matrix, and $\mathbf{T}_c \in \mathbb{C}^{M\times N}$ is a full Toeplitz matrix, which are defined as

$$\mathbf{T}_g = \begin{bmatrix} g_1 & 0 & \cdots & 0 \\ \vdots & g_1 & \ddots & \vdots \\ g_L & \vdots & \ddots & 0 \\ 0 & g_L & \ddots & g_1 \\ \vdots & \ddots & \ddots & \vdots \\ 0 & \cdots & 0 & g_L \end{bmatrix}, \quad \mathbf{T}_c = \begin{bmatrix} c_0 & c_{-1} & \cdots & c_{-N+1} \\ c_1 & c_0 & \ddots & \vdots \\ \vdots & c_1 & \ddots & c_{-1} \\ c_{M-N} & \ddots & \ddots & c_0 \\ \vdots & \ddots & \ddots & c_1 \\ c_{M-1} & \cdots & \cdots & c_{M-N} \end{bmatrix}. \tag{8}$$

We assume that $\tilde{\mathbf{n}} \in \mathbb{C}^{M\times 1}$ is a zero-mean circularly symmetric complex Gaussian noise with covariance $\mathbf{\Sigma}_{\tilde{n}} = \mathtt{E}[\tilde{\mathbf{n}}\tilde{\mathbf{n}}^\dagger] = \sigma_{\tilde{n}}^2 \mathbf{I}_M$, where $\sigma_{\tilde{n}}^2$ is the noise variance. The scattering coefficients of clutter $\mathbf{c}$ are modeled as a zero-mean complex wide-sense stationary (WSS) Gaussian process with known covariance $\mathbf{\Sigma}_c \in \mathbb{H}^K$, which has a Toeplitz structure.

After $\tilde{\mathbf{y}}$ is acquired in the observation window, it is processed by the radar receiver by filtering [14] or symbol processing method [10] to detect the target in clutter and noise and estimate its range and velocity. The performance of a radar system is determined by the signal-to-clutter-plus-noise ratio (SCNR) as it affects the detection statistics and the estimation accuracy [14]. The SCNR is formulated as

$$\Psi(\tilde{\mathbf{x}}) = \frac{\mathtt{E}\left[\|\mathbf{T}_g \tilde{\mathbf{x}}\|^2\right]}{\mathtt{E}\left[\|\mathbf{T}_c \tilde{\mathbf{x}}\|^2\right] + \mathtt{E}\left[\|\tilde{\mathbf{n}}\|^2\right]} \tag{9}$$

which is the ratio of the reflected signal power from the target to the reflected power from the clutter plus additive noise power. As $\Psi(\tilde{\mathbf{x}})$ increases, the detection performance of the radar receiver improves as studied in [13] for the frequency domain representation. Thus, by designing the dual-use waveform, the detection and estimation performance can be improved based on available second-order statistics of the target and clutter (i.e., $\mathbf{\Sigma}_g$ and $\mathbf{\Sigma}_c$), respectively.

C. Communication Channel Model

The vehicular channel is modeled as a doubly-selective channel due to high mobility and multi-path propagation. But, the time-selectivity due to relative velocities can be ignored considering the maximum Doppler spread is low and the coherence time T_c is longer than symbol time T_s. Also, the channel is assumed to be invariant for a symbol duration and variant for longer periods where the change in the channel can be estimated via pilot symbols. By omitting the time-varying property, the FIR of the communication channel is given as

$\mathbf{h} = [h_1, h_2, \ldots, h_J]^T$, where each channel tap h_j is modeled as a complex Gaussian with zero-mean and variance of σ_h^2.

In matrix form, the received OFDM signal $\mathbf{z}$ is formulated as

$$\mathbf{z} = \mathbf{H}\mathbf{x} + \mathbf{n} \tag{10}$$

where $\mathbf{H} = \mathsf{Diag}(\mathbf{W}_{NJ}\mathbf{h}) = \mathsf{Diag}(H_0, H_1, ..., H_N)$ and $\mathbf{W}_{NJ}$ is the N-point DFT matrix with the size of $(N \times J)$. To decode the received symbols correctly and acquire the CSI, the communication receiver uses pilot symbols to estimate the channel's FIR $\mathbf{h}$ with a linear minimum mean squared error (LMMSE) estimator. The estimated channel FIR denoted with $\hat{\mathbf{h}}$ is sent back to the transmitter. Thus, the channel capacity with transmitter CSI is expressed as

$$\mathcal{C}(\mathbf{x}_d) = \sum_{i=1}^{N_d} \Delta f \log_2\left(1 + \frac{|x_{d,i}|^2 |\hat{H}_i|^2}{\sigma_n^2}\right). \tag{11}$$

To formulate the effective SNR and optimal power allocation between data and pilot subcarriers, we first derive the mean squared error (MSE) of the channel estimator. The received pilot symbols is expressed as

$$\mathbf{z}_p = \mathbf{H}_p(\mathbf{a}_p \odot \mathbf{p}) + \mathbf{n}_p = \mathbf{H}_p\mathbf{x}_p + \mathbf{n}_p \tag{12}$$

where $\mathbf{H}_p = \boldsymbol{\mathcal{P}}_p^T \mathbf{H} \boldsymbol{\mathcal{P}}_p$. This equation can be simplified as

$$\mathbf{z}_p = \mathbf{X}_p \boldsymbol{\mathcal{P}}_p^T \mathbf{W}_{NJ}\mathbf{h} + \mathbf{n} \tag{13}$$

where $\mathbf{X}_p = \mathsf{Diag}(\mathbf{x}_p)$ and $\mathbf{z}_p$ is the input of the channel estimator. According to [18], the LMMSE estimator of the channel with pilot input is

$$\hat{\mathbf{h}} = \frac{1}{\sigma_n^2}\left(\boldsymbol{\Sigma}_h^{-1} + \frac{1}{\sigma_n^2}\mathbf{W}_{pJ}^\dagger \mathbf{X}_p^\dagger \mathbf{X}_p \mathbf{W}_{pJ}\right)^{-1} \mathbf{W}_{pJ}^\dagger \mathbf{X}_p^\dagger \mathbf{z}_p \tag{14}$$

where $\boldsymbol{\Sigma}_\mathbf{h} = \mathtt{E}[\mathbf{h}\mathbf{h}^\dagger]$, $\mathbf{W}_{pJ} = \boldsymbol{\mathcal{P}}_p^T \mathbf{W}_{NJ}$ with size of $(N_p \times J)$ and estimation error is $\boldsymbol{\Theta}_h = \mathbf{h} - \hat{\mathbf{h}}$. The MSE of the LMMSE estimator is given in [18] as

$$\xi = \mathsf{tr}\Big(\mathtt{E}[\boldsymbol{\Theta}_h \boldsymbol{\Theta}_h^\dagger]\Big) = \mathsf{tr}\left(\left(\boldsymbol{\Sigma}_h^{-1} + \frac{1}{\sigma_n^2}\mathbf{W}_{pJ}^\dagger \mathbf{X}_p^\dagger \mathbf{X}_p \mathbf{W}_{pJ}\right)^{-1}\right). \tag{15}$$

The MSE is minimized, if $\mathtt{E}[\boldsymbol{\Theta}_h \boldsymbol{\Theta}_h^\dagger]$ in (15) is diagonal as proven in [19]. The matrix is diagonal if we allocate equal power to pilot symbols and place them equally spaced in frequency. Then, the MSE due to estimation error becomes

$$\xi = \frac{J\sigma_h^2 \sigma_n^2}{\sigma_n^2 + P_p \sigma_h^2}, \tag{16}$$

where $P_p = \mathbf{a}_p^\dagger \mathbf{a}_p$ is the total power allocated to pilot symbols. Imperfect channel estimation at the receiver reduces the effective communication SNR. Based on [19, (25)], effective SNR is expressed as

$$SNR_{eff} = \frac{P_d J\sigma_h^2 - P_d \xi}{P_d \xi + \sigma_n^2 N_d} \tag{17}$$

where $P_d = \mathbf{a}_d^\dagger \mathbf{a}_d$ is the total power allocated to data symbols in terms of ξ. After replacing (16) in (17) and taking the derivative, optimal power allocation parameter $\gamma = P_d/P_t$ is derived as

$$\gamma_{opt} = \frac{1}{1 + \sqrt{1 - \frac{(N_d - J)\sigma_h^2 P_t}{N_d P_t \sigma_h^2 + N_d \sigma_n^2}}} \tag{18}$$

where P_t is the total signal power equal to $P_d + P_p$. With CSI, the transmitter adjusts the total power allocated to data and pilot subcarriers according to $\gamma_{opt} = P_d/P_t$ to maximize effective SNR. Since equally powered pilot symbols achieve the minimum MSE, the total pilot power $P_p = (1 - \gamma_{opt})P_t$ is shared equally between pilot subcarriers.

III. Problem Formulation

In this section, we focus on designing an optimal dual-use waveform that maximizes the received radar SCNR. Thus, we aim to maximize (9) in terms of $\tilde{\mathbf{x}}$ while preserving the PSK modulation and meeting the requirements of the communication system. For communication, we want to minimize the MSE in channel estimation and maximize effective SNR with CSI at the transmitter. To maximize the effective SNR (17), the JARC system allocates power according to the optimal power allocation γ_{opt} derived in (18). Moreover, equally powered and spaced pilot symbols achieve minimum MSE for a given total power as explained in Section II-C. Based on this observation, we choose our permutation matrix $\boldsymbol{\mathcal{P}}_p$ to place pilots periodically in frequency and formulate a constraint in our design problem as

$$\left(\boldsymbol{\mathcal{P}}_p^T \mathbf{x}\right)^\dagger \odot \boldsymbol{\mathcal{P}}_p^T \mathbf{x} = \mathbf{x}_p^\dagger \odot \mathbf{x}_p = (1 - \gamma_{opt})P_t/N_p \tag{19}$$

to force equal power allocation. In addition, we allocate the remaining power to data symbols by

$$\left(\boldsymbol{\mathcal{P}}_d^T \mathbf{x}\right)^\dagger \boldsymbol{\mathcal{P}}_d^T \mathbf{x} = \mathbf{x}_d^\dagger \mathbf{x}_d = \gamma_{opt} P_t. \tag{20}$$

Regarding the performance metrics, we present the optimization problem for joint OFDM waveform design that maximizes the radar performance with communication performance constraints for channel estimation error and capacity. The optimization problem is formulated as

$$\begin{aligned} \max_{\tilde{\mathbf{x}} \in \mathbb{C}^{N\times 1}} \quad & \frac{\mathtt{E}\left[\tilde{\mathbf{x}}^\dagger \mathbf{T}_g^\dagger \mathbf{T}_g \tilde{\mathbf{x}}\right]}{\mathtt{E}\left[\tilde{\mathbf{x}}^\dagger \mathbf{T}_c^\dagger \mathbf{T}_c \tilde{\mathbf{x}}\right] + \mathtt{E}\left[\tilde{\mathbf{n}}^\dagger \tilde{\mathbf{n}}\right]}, \\ \text{s.t.} \quad & \mathtt{C}_1 : \mathcal{C}(\mathbf{x}_d) \geq r_{min}, \\ & \mathtt{C}_2 : \mathbf{x}_d^\dagger \mathbf{x}_d = \gamma_{opt} P_t, \\ & \mathtt{C}_3 : \mathbf{x}_p^* \odot \mathbf{x}_p = (1 - \gamma_{opt})P_t/N_p \\ & \mathtt{C}_4 : \mathbf{x}^* \odot \mathbf{x} \preceq \mathbf{d}, \end{aligned} \tag{P1}$$

where r_{min} in $\mathtt{C}_1$ is the minimum channel capacity requirement for (11), $\mathtt{C}_2$ is the power allocation for data symbols, and $\mathtt{C}_3$ ensures the equal power allocation for pilot symbols for accurate channel estimation. Also, $\mathbf{d} \in \mathbb{R}_{\geq 0}^{N\times 1}$ is the power constraint on each frequency band to comply with maximum transmit power limitations.

Notice that the optimization variable $\tilde{\mathbf{x}}$ contains PSK modulated complex symbols $\mathbf{s}$ for communication as shown in

(2). Since each symbol in $\mathbf{s}$ has unit-energy with phase modulation, we design complex coefficients in $\mathbf{a}$ by restricting their phase according to the phase of symbols in $\mathbf{s}$. Therefore, we introduce phase constraints to allow the communication receiver to demodulate received symbols correctly without the knowledge of $\mathbf{a}$. Hence, we reformulate (P1) as

$$\begin{aligned} \max_{\mathbf{a}\in\mathbb{C}^{N\times 1}} \quad & \frac{\mathbf{a}^\dagger \mathbf{Q}_{gs}\mathbf{a}}{\mathbf{a}^\dagger \mathbf{Q}_{cs}\mathbf{a}+\sigma_n^2 M}, \\ \text{s.t.} \quad & \mathtt{C}_1 : \mathcal{C}(\mathbf{a}_d) \geq r_{min}, \\ & \mathtt{C}_2 : \mathbf{a}^\dagger\mathbf{a} = P_t, \\ & \mathtt{C}_3 : \mathbf{a}_p^* \odot \mathbf{a}_p = P_p/N_p, \\ & \mathtt{C}_4 : \mathbf{a}^* \odot \mathbf{a} \preceq \mathbf{d}, \\ & \mathtt{C}_5 : \mathsf{arg}(a_n) \in [-\theta/2, \theta/2],\ n = 1,\ldots,N, \end{aligned} \tag{P2}$$

where θ is the maximum allowed phase range. The matrices in the objective function are defined as $\mathbf{Q}_{gs} = \mathbf{W}_N \mathtt{E}[\mathbf{T}_g^\dagger \mathbf{T}_g]\mathbf{W}_N^\dagger \odot \mathtt{E}[\mathbf{s}\mathbf{s}^\dagger]^*$ and $\mathbf{Q}_{cs} = \mathbf{W}_N \mathtt{E}[\mathbf{T}_c^\dagger \mathbf{T}_c]\mathbf{W}_N^\dagger \odot \mathtt{E}[\mathbf{s}\mathbf{s}^\dagger]^*$.

For this problem, we consider two cases: the coefficients of $\mathbf{a}$ are designed (i) with *zero-phase constraints* (i.e., $\theta = 0$) which is the domain of non-negative real numbers $\mathbb{R}_{\geq 0}^{N\times 1}$ and (ii) with *non-zero phase constraints* (i.e., $\theta \in [0, 2\pi)$). (P2) is a Quadratically Constrained Quadratic Fractional Programming (QCQFP) problem with a sum of logarithms constraint in $\mathtt{C}_1$ and phase constraint in $\mathtt{C}_5$. It is a non-convex problem due to the maximization of the ratio of two convex quadratic functions. Thus, obtaining a globally optimal solution is difficult to achieve efficiently. Thus, we propose relaxation and approximation methods to recast (P2) as a convex problem. Then, we resort to interior-point algorithms to obtain near-optimal solutions in polynomial time as evaluated in [20] for convex second-order cone programming (SOCP) and semidefinite programming (SDP) problems.

IV. Semidefinite Relaxation Method for $\theta = 0$

In this section, we formulate and solve (P2) as an SDP problem based on the semidefinite relaxation (SDR) method. The SDR method is studied for different NP-hard and non-convex problems in literature [21] to obtain near optimal solutions efficiently. It is also evaluated for Boolean quadratic programming (BQP) and non-convex quadratically constrained quadratic programming (QCQP) problems in [22].

The SDP formulation relies on the fact that quadratic functions of $\mathbf{a}$ are linear in the matrix $\mathbf{A} = \mathbf{a}\mathbf{a}^\dagger$ and can be expressed with trace operations,i.e., $\mathbf{a}^\dagger\mathbf{Q}\mathbf{a} = \mathsf{tr}\big(\mathbf{Q}\mathbf{A}\big)$. To cast (P2) as an SDP problem, we change the optimization variable to $\mathbf{A} = \mathbf{a}\mathbf{a}^\dagger$ as

$$\begin{aligned} \max_{\mathbf{A}\in\mathbb{R}^{N\times N}} \quad & \frac{\mathsf{tr}\big(\mathbf{Q}_{gs}\mathbf{A}\big)}{\mathsf{tr}\big(\mathbf{Q}_{cs}\mathbf{A}\big)+\sigma_n^2 M}, \\ \text{s.t.} \quad & \mathtt{C}_1 : \mathcal{C}\big(\boldsymbol{\alpha}_d^{\odot 1/2}\big) \geq r_{min}, \\ & \mathtt{C}_2 : \mathsf{tr}(\mathbf{A}) = P_t, \\ & \mathtt{C}_3 : \boldsymbol{\mathcal{P}}_p^T \mathsf{diag}(\mathbf{A}) = P_p/N_p, \\ & \mathtt{C}_4 : \mathsf{diag}(\mathbf{A}) \preceq \mathbf{d}, \\ & \mathtt{C}_5 : \mathbf{A} \succeq 0,\ \mathtt{C}_6 : \mathsf{rank}(\mathbf{A}) = 1 \end{aligned} \tag{P3}$$

where $\boldsymbol{\alpha}_d = \boldsymbol{\mathcal{P}}_d^T \mathsf{diag}(\mathbf{A})$. The rank-one constraint in $\mathtt{C}_6$ is equivalent to $\mathbf{A} = \mathbf{a}\mathbf{a}^\dagger$, which is a non-convex constraint. The SDR method is employed by dropping the rank-one constraint to obtain a relaxed convex SDP problem.

However, the objective function of (P3) is still a fractional function (i.e., quasilinear) and the sum of logarithms constraint $\mathtt{C}_1$ is not an SDP constraint. Thus, we first reformulate $\mathtt{C}_1$ as

$$\mathcal{C}_{gm}(\boldsymbol{\alpha}_d) = \left(\prod_{i=1}^{N_d}\Big[1+\alpha_{d,i}\lambda_{h,i}\Big]\right)^{\frac{1}{N_d}} \geq 2^{c_{min}/N_d} \tag{21}$$

where $c_{min} = r_{min}/\Delta f$ and $\lambda_{h,i} = |\hat{H}_i|^2/\sigma_n^2$. In fact, $\mathcal{C}_{gm}$ in (21) is the geometric mean formulation of the function in (11). Since (21) is a product of nonnegative affine functions, $\mathtt{C}_1$ of (P3) can be recast as a second-order cone constraint similar to formulation in [23, Section 2.3]. Moreover, a second-order cone constraint can be expressed as a linear matrix inequality (LMI) and can be converted into an SDP constraint using the Schur complement lemma [23].

Next, we want to formulate the objective function of (P3) as a convex function while preserving the convexity of constraints. The Charnes-Cooper transformation is proposed in [24] to eliminate quasilinear objective function by formulating the linear fractional programming (LFP) problems as linear programming (LP) problems. Inspired by the Charnes-Cooper transformation, we change variable $\mathbf{B} = \mu\mathbf{A}$ where $\mu \in \mathbb{R}_{\geq 0}$ is an auxiliary variable that satisfies $\mathsf{tr}\big(\mathbf{Q}_{cs}\mathbf{A}\big) + \sigma_n^2 M = 1/\mu$. Hence, we have a relaxed convex SDP problem as

$$\begin{aligned} \max_{\substack{\mathbf{B}\in\mathbb{R}^{N\times N}\\ \mu\in\mathbb{R}}} \quad & \mathsf{tr}\big(\mathbf{Q}_{gs}\mathbf{B}\big), \\ \text{s.t.} \quad & \mathtt{C}_1 : \mathcal{C}_{gm,\mu}\big(\boldsymbol{\beta}_d, \mu\big) \geq \mu 2^{c_{min}/N_d} \\ & \mathtt{C}_2 : \mathsf{tr}(\mathbf{B}) = \mu P_t, \\ & \mathtt{C}_3 : \boldsymbol{\mathcal{P}}_p^T \mathsf{diag}(\mathbf{B}) = \mu(P_p/N_p), \\ & \mathtt{C}_4 : \mathsf{diag}(\mathbf{B}) \preceq \mu\mathbf{d}, \\ & \mathtt{C}_5 : \mathbf{B} \succeq 0, \\ & \mathtt{C}_6 : \mathsf{tr}\big(\mathbf{Q}_{cs}\mathbf{B}\big) + \mu\sigma_n^2 M = 1,\ \mathtt{C}_7 : \mu \geq 0 \end{aligned} \tag{P4}$$

where $\boldsymbol{\beta}_d = \boldsymbol{\mathcal{P}}_d^T \mathsf{diag}(\mathbf{B})$. With the change of variable, $\mathtt{C}_1$ of (P4) is redefined as

$$\mathcal{C}_{gm,\mu}(\boldsymbol{\beta}_d, \mu) = \left(\prod_{i=1}^{N_d}\Big[\mu+\beta_{d,i}\lambda_{h,i}\Big]\right)^{\frac{1}{N_d}} \geq \mu 2^{c_{min}/N_d} \tag{22}$$

which is the equivalent of $\mathtt{C}_1$ of (P3) with auxiliary μ.

(P4) is the relaxed convex SDP formulation of the original problem in (P2) for $\theta = 0$. The convex SDP problems can be solved in polynomial-time using interior-point algorithms [22]. As we obtain the optimal solution $(\mathbf{B}^\star, \mu^\star)$ for (P4), $\mathbf{A}^\star = \mathbf{B}^\star/\mu^\star$ is the solution for (P3) neglecting the rank-one constraint. Since the optimization variable $\mathbf{a}$ is in the non-negative domain $\mathbb{R}_{\geq 0}^{N\times 1}$ for this problem, we can extract the optimal vector by $\mathbf{a}^\star = \mathsf{diag}(\mathbf{A}^\star)^{\odot 1/2}$. However, we drop the rank-one constraint $\mathtt{C}_6$ of (P3) for the relaxation. Hence, if obtained $\mathbf{A}^\star$ is not rank-one, then it is a suboptimal solution to the original problem. Otherwise, it is an optimal solution.

V. Circulant Approximation (CA) Method for $\theta = 0$

Although the interior-point algorithms solve the convex SDP problem (P4) in polynomial time, the time complexity is still high due to the exponential increase in the dimension of SDP variables and constraints. Moreover, the SDR approach does not guarantee to find a low-rank result as it has been proven in [22] that the interior-point algorithms will return a higher rank solution. Thus, we need more time-efficient approaches.

In this section, we show that quadratic fractional function with Toeplitz matrices can be formulated as linear fractional function. Hence, we can formulate (P2) with a linear objective function and constraints and a geometric mean constraint (22) by using the Charnes-Cooper transformation. With this approach, our goal is to reduce the number of variables by exploiting the Toeplitz structure of $\boldsymbol{\mathcal{T}}_g = \mathtt{E}[\mathbf{T}_g^\dagger \mathbf{T}_g]$ and $\boldsymbol{\mathcal{T}}_c = \mathtt{E}[\mathbf{T}_c^\dagger \mathbf{T}_c]$ which are contained in $\mathbf{Q}_{gs}$ and $\mathbf{Q}_{cs}$ of (P2). For this formulation, we also assume that $\mathtt{E}[\mathbf{s}\mathbf{s}^\dagger] = \mathbf{I}_N$ by treating $\mathbf{s}$ as random with unit-energy symbols.

We first show that $\boldsymbol{\mathcal{T}}_g$ and $\boldsymbol{\mathcal{T}}_c$ are structured as Toeplitz matrices.

Lemma 1. *$\boldsymbol{\mathcal{T}}_g = \mathtt{E}[\boldsymbol{T}_g^\dagger \boldsymbol{T}_g]$ is structured as a Toeplitz matrix for a given lower Toeplitz matrix $\boldsymbol{T}_g \in \mathbb{C}^{M\times N}$.*

Proof. A complex square Toeplitz matrix $\boldsymbol{\mathcal{T}} \in \mathbb{C}^{N\times N}$ can be defined by a vector $\boldsymbol{\tau} \in \mathbb{C}^{(2N-1)\times 1}$ whose entries τ_i correspond to i^{th} diagonal elements. Since $\mathbf{T}_g$ is a lower triangular Toeplitz matrix, $\mathbf{T}_g^\dagger \mathbf{T}_g$ is a Toeplitz matrix defined by $\boldsymbol{\tau}_g = \mathbf{g}_{zp} * \mathbf{g}_{zp}^*$, where $\mathbf{g}_{zp}$ is the zero-padded $\mathbf{g}$ of length N given in (8). Thus, its expectation $\boldsymbol{\mathcal{T}}_g$ is also a Toeplitz matrix defined by $\boldsymbol{\tau}'_g$, whose entries are

$$\tau'_{g,i} = \mathsf{tr}\big(\Lambda_i \boldsymbol{\Sigma}_g\big), \quad i = -L+1, \ldots, L-1 \tag{23}$$

and zeros elsewhere, where Λ_i is a Toeplitz matrix with ones in i^{th} diagonal and zero elsewhere. □

Unlike $\mathbf{T}_g^\dagger \mathbf{T}_g$, one can observe that $\mathbf{T}_c^\dagger \mathbf{T}_c$ is not a Toeplitz matrix but its expectation is structured as Toeplitz.

Lemma 2. *$\boldsymbol{\mathcal{T}}_c = \mathtt{E}[\boldsymbol{T}_c^\dagger \boldsymbol{T}_c]$ is a Toeplitz matrix for a given Toeplitz matrix $\boldsymbol{T}_c \in \mathbb{C}^{M\times N}$ whose coefficients are modeled as a zero-mean complex WSS process.*

Proof. Its entries $e_{m,n}$ are equal to $\mathbf{c}_m^\dagger \mathbf{c}_n$, where $\mathbf{c}_n$ is the n^{th} column vector of $\mathbf{T}_c$ as in (8). Since $\boldsymbol{\Sigma}_c$ is structured as a Toeplitz matrix, the expectation of each element $\mathtt{E}[e_{m,n}]$ in i^{th} diagonal (i.e., $n-m=i$) are equal and calculated as

$$\tau_{c,i} = M\sigma_{c,i}, \quad i = -N+1, \ldots, N-1 \tag{24}$$

where $\sigma_{c,i}$ is the i^{th} diagonal element of $\boldsymbol{\Sigma}_c$. □

While Toeplitz matrices are extensively used in signal processing and information theory, its special instance called the circulant matrices provides a more structured form that can be diagonalized by the DFT matrix [25]. Furthermore, it has been shown in [26] that a Toeplitz matrix $\boldsymbol{\mathcal{T}}$ can be approximated into circulant form $\boldsymbol{\mathcal{C}}$ in the sense of minimizing $\|\boldsymbol{\mathcal{T}} - \boldsymbol{\mathcal{C}}\|_F$. It is proved that these matrices are asymptotically equivalent in terms of eigenvalues. Hence, we follow the circulant approximation method for $\boldsymbol{\mathcal{T}}_g$ and $\boldsymbol{\mathcal{T}}_c$ in which row entries are defined by

$$\nu_i = \frac{(N-k)\tau_i + i\tau_{-(n-i)}}{N}, \quad i = 0, \ldots, N-1. \tag{25}$$

for circulant approximations as $\boldsymbol{\mathcal{C}}_g$ and $\boldsymbol{\mathcal{C}}_c$, respectively. Since circulant matrices are diagonalizable with the DFT matrix, the objective function in (P2) is formulated as

$$\begin{aligned}\frac{\mathbf{a}^\dagger W_N \boldsymbol{\mathcal{C}}_g W_N^\dagger \mathbf{a}}{\mathbf{a}^\dagger W_N \boldsymbol{\mathcal{C}}_c W_N^\dagger \mathbf{a} + \sigma_n^2 M} &= \frac{\mathbf{a}^\dagger \boldsymbol{\Lambda}_g \mathbf{a}}{\mathbf{a}^\dagger \boldsymbol{\Lambda}_c \mathbf{a} + \sigma_n^2 M} \\ &= \frac{\boldsymbol{\lambda}_g^T \boldsymbol{\alpha}}{\boldsymbol{\lambda}_c^T \boldsymbol{\alpha} + \sigma_n^2 M},\end{aligned} \tag{26}$$

where $\boldsymbol{\lambda} = \mathsf{diag}(\boldsymbol{\Lambda})$ which are real diagonal matrices and $\boldsymbol{\alpha} = \mathbf{a}^{\odot 2}$. Now, we reformulate (P2) as

$$\begin{aligned}\max_{\boldsymbol{\alpha}\in\mathbb{R}_{\geq 0}^{N\times 1}} \quad & \frac{\boldsymbol{\lambda}_g^T \boldsymbol{\alpha}}{\boldsymbol{\lambda}_c^T \boldsymbol{\alpha} + \sigma_n^2 M}, \\ \text{s.t.} \quad & \mathtt{C}_1 : \mathcal{C}\big(\boldsymbol{\alpha}_d^{\odot 1/2}\big) \geq r_{min}, \\ & \mathtt{C}_2 : \sum_{i=1}^{N} \alpha_i = P_t, \\ & \mathtt{C}_3 : \boldsymbol{\alpha}_p = P_p/N_p, \\ & \mathtt{C}_4 : \boldsymbol{\alpha} \preceq \mathbf{d},\end{aligned} \tag{P5}$$

which is a quasiconvex problem with a quasilinear objective function, linear constraints $\mathtt{C}_{2-4}$ and a convex nonlinear capacity constraint $\mathtt{C}_1$. Similar to the SDR approach, we resort to the Charnes-Cooper transformation to eliminate the quasilinear objective function. Thus, we change variable $\boldsymbol{\beta} = \mu\boldsymbol{\alpha}$ to cast the problem as

$$\begin{aligned}\max_{\substack{\boldsymbol{\beta}\in\mathbb{R}_{\geq 0}^{N\times 1} \\ \mu\in\mathbb{R}}} \quad & \boldsymbol{\lambda}_g^T \boldsymbol{\beta}, \\ \text{s.t.} \quad & \mathtt{C}_1 : \mathcal{C}_{gm,\mu}\big(\boldsymbol{\beta}_d, \mu\big) \geq \mu 2^{c_{min}/N_d}, \\ & \mathtt{C}_2 : \sum_{i=1}^{N} \beta_i = \mu P_t, \\ & \mathtt{C}_3 : \boldsymbol{\beta}_p = \mu P_p/N_p, \\ & \mathtt{C}_4 : \boldsymbol{\beta} \preceq \mu\mathbf{d}, \\ & \mathtt{C}_5 : \boldsymbol{\lambda}_c^T \boldsymbol{\beta} + \mu\sigma_n^2 M = 1, \ \mathtt{C}_6 : \mu \geq 0\end{aligned} \tag{P6}$$

where $c_{min} = r_{min}/\Delta f$ and μ is an auxiliary variable similar to (P4) that satisfies $\boldsymbol{\lambda}_c^T \boldsymbol{\alpha} + \sigma_n^2 M = 1/\mu$.

The problem in (P6) is a convex SDP problem with a linear objective function, linear constraints $\mathtt{C}_{2-6}$, and a geometric mean constraint $\mathtt{C}_1$, which can be formulated as a SOCP/SDP constraint. Compared to (P4), the dimension of variables and constraints are reduced and do not increase exponentially due to the linear formulation of the objective function with the circulant approximation. To find the optimal solution $(\boldsymbol{\beta}^\star, \mu^\star)$ for (P6), we also use the interior-point algorithm. The optimal solution $\boldsymbol{\alpha}^\star$ of (P5) is computed by $\boldsymbol{\alpha}^\star = \boldsymbol{\beta}^\star/\mu^\star$. Since $\mathbf{a}$ is a non-negative real vector, we can compute the optimal coefficients as $a_i = \sqrt{\alpha_i}, \ \forall i \in \{1, \ldots, N\}$.

VI. Waveform Design with Phase Constraints

With the SDR and CA methods, we solve the problem that is originally defined in the complex domain without the phase constraint $\mathtt{C}_5$ (i.e., $\theta = 0$). Thus, we design the optimal coefficients in $\mathbf{a}$ as power allocation coefficients without disturbing the phase modulation of complex communication symbols in $\mathbf{s}$. However, we can extend the feasible region of the problem by designing the coefficients of $\mathbf{a}$ in complex domain and increase the maximum achievable SCNR. Nevertheless, we need to consider the phase shift due to data modulation.

In this section, we solve the original problem in (P1) with the phase constraint. Without the phase constraint, it is been shown that complex quadratic problem is NP-hard [27]. In radar literature, similar phase constraints are introduced as 'similarity constraint' to design radar codes that are similar to a prefixed sequence. In [15], a method based on the SDR and Gaussian randomization is proposed to design constant modulus radar codes with a similarity constraint. The Gaussian randomization procedure [22] is employed to generate random codes by using the SDR solution as a covariance matrix. However, an excessive number of random samples are required to acquire a near-optimal solution, because randomly generated codes requires scaling for feasibility as pointed out in [28].

In this section, we propose a two-stage approach for the original problem under phase constraint in (P2) by exploiting the solution acquired with the CA method. As shown in (P4), the quadratic functions and constraints can be linearized with the SDP formulation and the Charnes-Cooper transformation. However, the linear phase constraint $\mathtt{C}_5$ in (P2), which is a QCQFP, complicates the linear formulation with the SDR.

In Section V, we show that power coefficients $\boldsymbol{\alpha}$ can be found efficiently in the real domain. In the first stage, we assume that $\theta = 0$ and find optimal $\boldsymbol{\alpha}^\star \in \mathbb{R}_{\geq 0}^{N\times 1}$ by solving the problem in the real domain with the CA method. With $\boldsymbol{\alpha}^\star$, we have a feasible power allocation for each subcarrier that satisfies constraints $\mathtt{C}_{1-4}$ of (P2). Hence, we simplify the original problem by changing the domain as

$$\begin{aligned} \max_{\mathbf{u}\in\mathbb{C}^{N\times 1}} \quad & \frac{\mathbf{u}^\dagger \mathbf{Q}_{ga}\mathbf{u}}{\mathbf{u}^\dagger \mathbf{Q}_{ca}\mathbf{u} + \sigma_n^2 M}, \\ \text{s.t.} \quad & \mathtt{C}_1 : |u_n| = 1, \\ & \mathtt{C}_2 : \mathsf{arg}(u_n) \in [\phi_n - \theta/2, \phi_n + \theta/2], \end{aligned} \tag{P7}$$

where $n = 1, \ldots, N$ and ϕ_n is the phase of communication symbol in the n^{th} subcarrier. The matrices in the objective function are defined as $\mathbf{Q}_{ga} = \mathbf{W}_N \mathsf{E}[\mathbf{T}_g^\dagger \mathbf{T}_g]\mathbf{W}_N^\dagger \odot \mathsf{Diag}(\boldsymbol{\alpha}^\star)$ and $\mathbf{Q}_{ca} = \mathbf{W}_N \mathsf{E}[\mathbf{T}_c^\dagger \mathbf{T}_c]\mathbf{W}_N^\dagger \odot \mathsf{Diag}(\boldsymbol{\alpha}^\star)$.

Notice that the domain of coefficients in $\mathbf{u}$ is restricted to the unit circle, where the feasible region is defined according to the phase of each communication symbol. In other words, we choose the best possible communication symbols in the feasible region to maximize the SCNR of the radar. (P7) is a non-convex problem due to the unit modulus constraint $\mathtt{C}_1$ and the maximization of convex quadratic fractional function. To formulate (P7) as an SDP, we first express $\mathtt{C}_2$ equivalently as

$$\mathtt{C}_2 : \mathsf{Re}(\mathbf{u} \odot \mathbf{s}^*) \succeq \cos(\theta/2), \tag{27}$$

in the vector form. We introduce three variables $\boldsymbol{\Upsilon} = \mu\mathbf{u}\mathbf{u}^\dagger$, $\boldsymbol{\upsilon} = \mu\mathbf{u}$, and μ. Thus, we formulate (P7) equivalently as

$$\begin{aligned} \max_{\substack{\boldsymbol{\Upsilon}\in\mathbb{C}^{N\times N} \\ \boldsymbol{\upsilon}\in\mathbb{C}^{N\times 1} \\ \mu\in\mathbb{R}}} \quad & \mathsf{tr}\big(\mathbf{Q}_{ga}\boldsymbol{\Upsilon}\big), \\ \text{s.t.} \quad & \mathtt{C}_1 : \mathsf{diag}\big(\boldsymbol{\Upsilon}\big) = \mu, \\ & \mathtt{C}_2 : \mathsf{Re}(\boldsymbol{\upsilon} \odot \mathbf{s}^*) \succeq \mu\cos(\theta/2), \\ & \mathtt{C}_3 : \mathsf{tr}\big(\mathbf{Q}_{ca}\boldsymbol{\Upsilon}\big) + \mu\sigma_n^2 M = 1, \\ & \mathtt{C}_4 : \Gamma := \begin{bmatrix} \boldsymbol{\Upsilon} & \boldsymbol{\upsilon} \\ \boldsymbol{\upsilon}^\dagger & \mu \end{bmatrix} = 0, \end{aligned} \tag{P8}$$

where $\mathtt{C}_4$ is a non-convex LMI constraint that is the equivalent of $\boldsymbol{\Upsilon} - \boldsymbol{\upsilon}\boldsymbol{\upsilon}^\dagger/\mu = 0$ using the Schur complement.

The SDR is applied by replacing the non-convex equality constraint $\mathtt{C}_4$ with its convex relaxation $\Gamma \succeq 0$. Hence, we have a convex SDP problem which is solved by the interior-point method to obtain near-optimal $\boldsymbol{\upsilon}^\star$. Then, the optimal communication symbol $u_n^\star$ for (P7) is acquired by $u_n^\star = \upsilon_n^\star/(\mu|\upsilon_n^\star|)$ in which the coefficients are normalized for feasibility. Therefore, the optimal coefficients for the original problem (P2) are defined by $a_n^\star = \sqrt{\alpha_n^\star}u_n^\star/s_n$ for given communication symbols s_n.

VII. Numerical Results

In this section, we evaluate the performance of the proposed methods to design complex coefficients of the joint OFDM waveform as expressed in (P2) in terms of time complexity and obtained SCNR values. For the time complexity simulations, the number of subcarriers N is the main parameter that affects the performance of proposed approaches. Since the original problem is non-convex, the proposed methods rely on relaxation and approximation approaches to find near-optimal solutions. Thus, we also compare the objective values obtained by the proposed methods with the baseline performance that is achieved with equal power allocation.

The dual-use system operates in 77 GHz mmWave automotive radar spectrum with the bandwidth of 1 GHz which achieves the range resolution of $\Delta R = 0.15$ m. The number of pilot subcarriers is $N_p = N/8$ and total transmit power is determined by $P_t = 10\log_{10}(N)$ dB. With given configuration and $N = 256$ subcarriers, we can achieve data rates *up to 1 Gbps* with *unencoded OFDM signal* that uses quadrature phase-shift keying (QPSK) modulation and guard interval of 1/4. Moreover, the communication channel is modeled with $J = 7$ taps whose coefficients are generated as i.i.d Rayleigh fading with variance $\sigma_h^2 = 1$ and the total power gain is normalized to 16 dB. We assume that the radar target is a vehicle modeled as an extended target with $L = 7$ scatterers resolved in range. The target covariance $\boldsymbol{\Sigma}_g$ is randomly generated with the total reflecting power of $\mathsf{tr}(\boldsymbol{\Sigma}_g) = 25$ dB. The variance of the additive thermal noise is $\sigma_n^2 = 1$.

Based on given parameters, the optimal power allocation parameter γ_{opt} is calculated as in (20) for the transmitter. The minimum capacity requirement r_{min} is determined by the capacity achieved by the equal power allocated waveform which is the baseline strategy for unknown target and clutter. Thus, the SCNR optimal waveform should achieve the capacity of equal power allocation.

The problems in this work are formulated as convex SDP problems which can be solved efficiently with interior-point algorithms. Thus, we use the convex optimization toolbox CVX [29] in MATLAB that implements an interior-point algorithm called SDPT3 [30] for SDP problems. We run simulations on a PC that is equipped with Intel Core i7-6700HQ@2.60 GHz processor and 16 GB RAM.

A. Achieved SCNR Values

We first evaluate the performance of proposed approach in terms of achieved objective values which is SCNR. While the baseline value is the SCNR for the equal power allocated waveform ($\theta = 0$), the upper bound is the optimal solution of (P2) without the phase constraint, which is the equivalent to $\theta = 2\pi$. Without the phase constraint, (P2) is solved for $\mathbf{A} \in \mathbb{C}^N$ in the complex domain using the SDR approach given in Section IV. For the simulations, the total reflected power from the clutter is chosen as the control parameter. The clutter covariance $\mathbf{\Sigma}_c$ is generated randomly as a positive definite Toeplitz matrix due to its WSS property. We use different reflecting powers for clutter as $\mathrm{tr}(\mathbf{\Sigma}_c) \in \{5, 8, 11, 14, 17\}$ dB while the target's response and total transmit power are fixed.

In Fig. 2, the achieved SCNR values are shown for the SDR, CA with $\theta = 0$ and, phase constrained design (PCD) with $\theta = \pi/6$. As shown in the figure, the waveform design approaches can improve the SCNR compared to equal power allocation. As the radar estimation accuracy is scaling with $1/\sqrt{SCNR}$ [14], the optimal waveform can improve the accuracy by approximately 20% over the baseline performance. The improvement also depends on the response of the target and clutter. If the target's response has deep fades over certain frequency bands, then the improvement with the adaptive waveform would be greater compared to a frequency-flat response. Fig. 4 is the zoomed version of Fig. 2 with the clutter power of 8 dB. We also add additional results for the

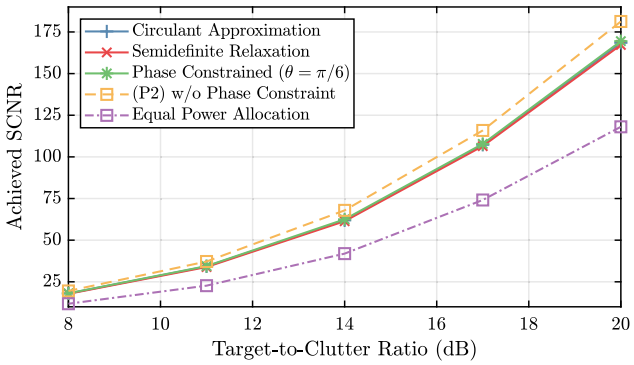

Fig. 2. Obtained SCNR values with proposed methods

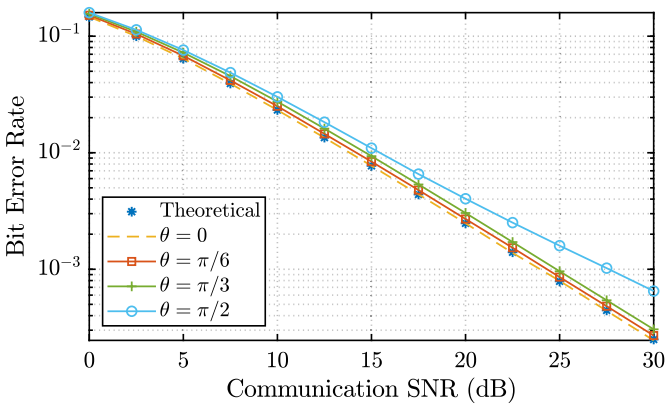

Fig. 3. Achieved bit error rates for different phase constraints.

PCD approach with different phase constraint values θ. Notice that the SDR approach performs worse than CA for $\theta = 0$. The reason is that the SDR approach gives suboptimal results due to the removal of the rank-one constraint. As explained in [22], the interior-point algorithm returns higher rank solutions which are suboptimal.

Furthermore, relaxing the phase constraint with non-zero θ values can increase the achieved SCNR. However, the improvement is limited for lower θ values and increasing θ degrades the communication performance due to reduced distance between constellations. The degradation is observed for bit error rate (BER) performances. Fig. 3 shows the achieved BER values for waveforms designed with different phase constraints. Since QPSK is used, the increase in BER is low for $\theta < \pi/2$ compared to $\theta = 0$ but increases as $\theta \geq \pi/2$

B. Time Complexity

For the time complexity evaluations, the clutter covariance is $\mathbf{\Sigma}_c$ is randomly generated as a Toeplitz matrix due to its WSS property with the total reflecting power of $\mathrm{tr}(\mathbf{\Sigma}_c) = 15$ dB. The total running times are measured to solve (P2) with the SDR, CA for $\theta = 0$ and with the PCD approach for $\theta = \pi/6$. For the PCD approach the total time is the sum of time required for the CA approach and the time measured to solve (P7). The measured time complexities are shown in Fig. 5 for different number of subcarriers $N \in \{32, 64, 128, 256\}$. As shown, the complexity increases exponentially due to matrix

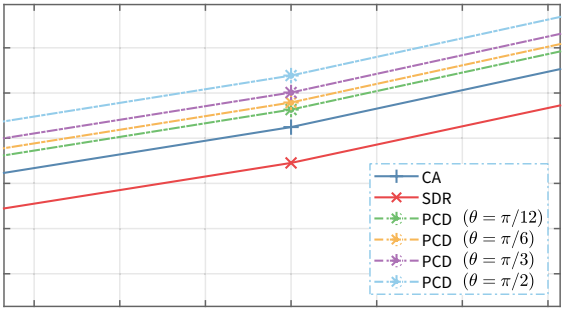

Fig. 4. Zoomed version of Fig. 2 with additional phase constraints

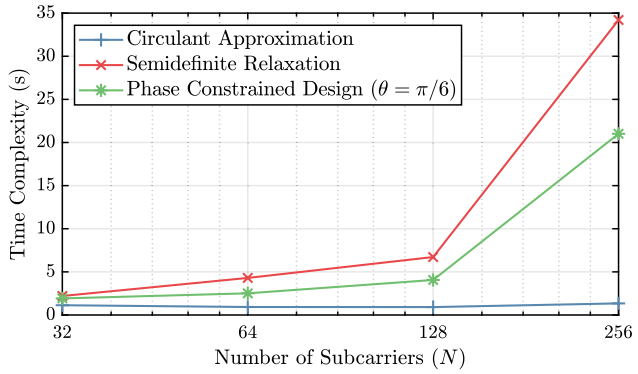

Fig. 5. Time complexity results for proposed methods

variables used in SDR and PCD. Fig. 6 shows the time complexity improvement of the CA approach over the SDR approach. We can see that the CA approach solves the problem around 20× and 100× faster for 256 and 512 subcarriers, respectively. In [31], it is shown that field-programmable gate arrays (FPGAs) can solve interior point algorithms 6.5× faster than CPUs. Combined with the hardware implementation, the lower time complexity and affine formulation make the CA approach suitable for designing joint waveform adaptively on the orders of milliseconds.

VIII. Conclusion

In this work, we study an adaptive OFDM waveform design problem for joint automotive radar and communication systems with given statistics about the extended target and signal-dependent clutter. First, we investigate the power and subcarriers allocation between data and pilot symbols in the OFDM waveform to minimize the channel estimation error and formulate the effective channel capacity. Then, we present the design problem to maximize SCNR while maintaining baseline effective communication capacity compared to equal power allocated waveform. We show that the problem is a non-convex QCQFP and propose relaxation and approximation approaches for the problem. The numerical results show that the proposed CA approach solves the problem with good optimal value and low complexity compared to the well-known SDR approach. Our future work is to integrate peak-to-average power ratio (PAPR) constraint into our problem and extend this work with iterative linear approximation methods.

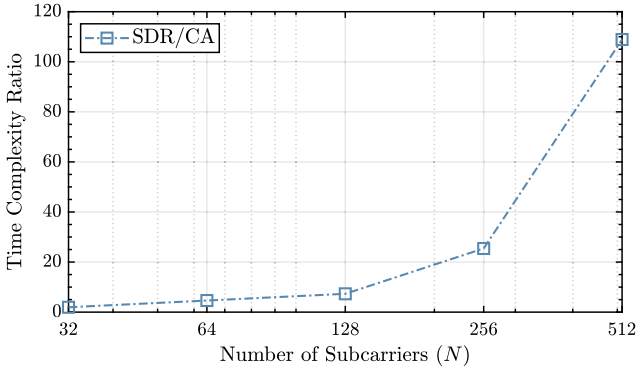

Fig. 6. Time complexity improvement over SDR with CA

References

[1] N. Lu, N. Cheng, N. Zhang, X. Shen, and J. W. Mark, "Connected vehicles: Solutions and challenges," *IEEE Internet of Things Journal*, vol. 1, no. 4, pp. 289–299, Aug 2014.

[2] R. Molina-Masegosa and J. Gozalvez, "Lte-v for sidelink 5g v2x vehicular communications: A new 5g technology for short-range vehicle-to-everything communications," *IEEE Vehicular Technology Magazine*, vol. 12, no. 4, pp. 30–39, Dec 2017.

[3] S. Kim, B. Qin, Z. J. Chong, X. Shen, W. Liu, M. H. Ang, E. Frazzoli, and D. Rus, "Multivehicle cooperative driving using cooperative perception: Design and experimental validation," *IEEE Transactions on Intelligent Transportation Systems*, vol. 16, no. 2, pp. 663–680, April 2015.

[4] J. Choi, V. Va, N. Gonzalez-Prelcic, R. Daniels, C. R. Bhat, and R. W. Heath, "Millimeter-wave vehicular communication to support massive automotive sensing," *IEEE Communications Magazine*, vol. 54, no. 12, pp. 160–167, December 2016.

[5] J. Hasch, E. Topak, R. Schnabel, T. Zwick, R. Weigel, and C. Waldschmidt, "Millimeter-wave technology for automotive radar sensors in the 77 ghz frequency band," *IEEE Transactions on Microwave Theory and Techniques*, vol. 60, no. 3, pp. 845–860, March 2012.

[6] A. Turlapaty and Y. Jin, "A joint design of transmit waveforms for radar and communications systems in coexistence," in *2014 IEEE Radar Conference*, May 2014, pp. 0315–0319.

[7] K.-W. Huang, M. Bică, U. Mitra, and V. Koivunen, "Radar waveform design in spectrum sharing environment: Coexistence and cognition," in *2015 IEEE Radar Conference (RadarCon)*, May 2015, pp. 1698–1703.

[8] P. Kumari, J. Choi, N. González-Prelcic, and R. W. Heath, "Ieee 802.11ad-based radar: An approach to joint vehicular communication-radar system," *IEEE Transactions on Vehicular Technology*, vol. 67, no. 4, pp. 3012–3027, April 2018.

[9] C. D. Ozkaptan, E. Ekici, O. Altintas, and C. Wang, "Ofdm pilot-based radar for joint vehicular communication and radar systems," in *2018 IEEE Vehicular Networking Conference (VNC)*, Dec 2018, pp. 1–8.

[10] C. Sturm and W. Wiesbeck, "Waveform design and signal processing aspects for fusion of wireless communications and radar sensing," *Proceedings of the IEEE*, vol. 99, no. 7, pp. 1236–1259, July 2011.

[11] Y. Han, E. Ekici, H. Kremo, and O. Altintas, "Optimal spectrum utilization in joint automotive radar and communication networks," in *2016 14th International Symposium on Modeling and Optimization in Mobile, Ad Hoc, and Wireless Networks (WiOpt)*, May 2016, pp. 1–8.

[12] F. Folster, H. Rohling, and U. Lubbert, "An automotive radar network based on 77 ghz fmcw sensors," in *IEEE International Radar Conference, 2005.*, May 2005, pp. 871–876.

[13] S. Kay, "Optimal signal design for detection of gaussian point targets in stationary gaussian clutter/reverberation," *IEEE Journal of Selected Topics in Signal Processing*, vol. 1, no. 1, pp. 31–41, June 2007.

[14] M. Richards, W. Holm, and J. Scheer, *Principles of Modern Radar: Basic Principles*, ser. Electromagnetics and Radar. Institution of Engineering and Technology, 2010.

[15] A. De Maio, S. De Nicola, Y. Huang, Z. Luo, and S. Zhang, "Design of phase codes for radar performance optimization with a similarity constraint," *IEEE Transactions on Signal Processing*, vol. 57, no. 2, pp. 610–621, Feb 2009.

[16] T. Guo and R. Qiu, "Ofdm waveform design compromising spectral nulling, side-lobe suppression and range resolution," in *2014 IEEE Radar Conference*, May 2014, pp. 1424–1429.

[17] P. Stoica, J. Li, and M. Xue, "Transmit codes and receive filters for radar," *IEEE Signal Processing Magazine*, vol. 25, no. 6, pp. 94–109, November 2008.

[18] S. M. Kay, *Fundamentals of Statistical Signal Processing: Estimation Theory*. Upper Saddle River, NJ, USA: Prentice-Hall, Inc., 1993.

[19] S. Ohno and G. B. Giannakis, "Capacity maximizing mmse-optimal pilots for wireless ofdm over frequency-selective block rayleigh-fading channels," *IEEE Transactions on Information Theory*, vol. 50, no. 9, pp. 2138–2145, Sept 2004.

[20] Y. Nesterov and A. Nemirovskii, *Interior-Point Polynomial Algorithms in Convex Programming*. Society for Industrial and Applied Mathematics, 1994.

[21] S. Boyd and L. Vandenberghe, "Semidefinite programming relaxations of non-convex problems in control and combinatorial optimization," 1997.

[22] Z. Luo, W. Ma, A. M. So, Y. Ye, and S. Zhang, "Semidefinite relaxation of quadratic optimization problems," *IEEE Signal Processing Magazine*, vol. 27, no. 3, pp. 20–34, May 2010.
[23] F. Alizadeh and D. Goldfarb, "Second-order cone programming," *Mathematical Programming*, vol. 95, no. 1, pp. 3–51, Jan 2003.
[24] A. Charnes and W. W. Cooper, "Programming with linear fractional functionals," *Naval Research Logistics Quarterly*, vol. 9, no. 3-4, pp. 181–186, 1962.
[25] R. M. Gray, "Toeplitz and circulant matrices: A review," *Foundations and Trends® in Communications and Information Theory*, vol. 2, no. 3, pp. 155–239, 2006.
[26] Z. Zhu and M. B. Wakin, "On the asymptotic equivalence of circulant and toeplitz matrices," *IEEE Transactions on Information Theory*, vol. 63, no. 5, pp. 2975–2992, May 2017.
[27] S. Zhang and Y. Huang, "Complex quadratic optimization and semidefinite programming," *SIAM Journal on Optimization*, vol. 16, no. 3, pp. 871–890, 2006.
[28] G. Cui, H. Li, and M. Rangaswamy, "Mimo radar waveform design with constant modulus and similarity constraints," *IEEE Transactions on Signal Processing*, vol. 62, no. 2, pp. 343–353, Jan 2014.
[29] M. Grant and S. Boyd, "CVX: Matlab software for disciplined convex programming, version 2.1," http://cvxr.com/cvx, Mar. 2014.
[30] K. C. Toh, M. J. Todd, and R. H. Tütüncü, "Sdpt3 — a matlab software package for semidefinite programming, version 1.3," *Optimization Methods and Software*, vol. 11, no. 1-4, pp. 545–581, 1999.
[31] J. L. Jerez, G. A. Constantinides, and E. C. Kerrigan, "An fpga implementation of a sparse quadratic programming solver for constrained predictive control," in *Proceedings of the 19th ACM/SIGDA International Symposium on Field Programmable Gate Arrays*, ser. FPGA '11. New York, NY, USA: ACM, 2011, pp. 209–218.